Construction and Building Materials 187 (2018) 699–707

Contents lists available at ScienceDirect

Construction and Building Materials

journal homepage: www.elsevier.com/locate/conbuildmat

Multi-functional properties of carbon nanofiber reinforced reactive powder concrete

Hui Wang [a], Xiaojian Gao [b,c,*], Junzhe Liu [a], Miao Ren [b], Anxun Lu [b]

[a] Faculty of Architectural, Civil Engineering and Environment, Ningbo University, 315000 Ningbo, China
[b] School of Civil Engineering, Harbin Institute of Technology, 150090 Harbin, China
[c] Key Lab of Structure Dynamic Behavior and Control (Harbin Institute of Technology), Ministry of Education, 150090 Harbin, China

HIGHLIGHTS

- Mechanical properties of CNF-RPC were presented.
- CNF-RPC showed excellent electrical and piezoresistive performances.
- CNF-RPC behaved a good deicing ability when CNFs contents reached 1.0%.

ARTICLE INFO

Article history:
Received 15 March 2018
Received in revised form 24 June 2018
Accepted 27 July 2018

Keywords:
Carbon nanofiber
Reactive powder concrete
Mechanical properties
Piezoresistivity
Deicing performance

ABSTRACT

This paper aimed to develop carbon nanofiber (CNF) reinforced reactive powder concrete (CNF-RPC) with multi-functional properties. Water to binder ratio (w/b) was kept at 0.2 and CNFs dosage ranged from 0% to 2% by volume of the total cementitious materials. Flexural and compressive strengths of CNF-RPC were determined for each dosage of CNFs. Piezoresistive performance of CNF-RPC was investigated while the piezoresistivity of CNFs added cement paste and mortar were also performed. Moreover, deicing performance of CNF-RPC was experimentally researched and numerally simulated using finite element analysis. Results indicated that RPC with appropriate content of CNFs performed favorable mechanical properties and excellent self-sensing performance. While CNFs content was close to the post-percolation threshold zone, CNF-RPC presented an obvious deicing performance. When CNFs content was in the percolation threshold zone, resistance of CNF-RPC rarely changed with measurement time. RPC containing CNFs (CNF-RPC) was more conductive and demonstrated a higher sensitivity and linearity of self-sensing performance than CNFs added cement paste and mortar samples.

1. Introduction

Reactive powder concrete (RPC) is produced with the maximum compactness theory. Quartz sand with optimized particle size distribution is used as fine aggregate instead of coarse aggregate and ordinary river sand. RPC usually contains a high percentage of mineral admixtures [1]. The mineral admixture can enhance the activity of RPC matrix, thus increasing the compactness of multi-size particle system. Therefore, RPC presents ultra-high strength, high toughness and excellent durability [1,2].

RPC matrix filled with conductive fillers can serve as multi-functional materials [3,4]. Multi-functional RPC with ultra-high strength can be used as concrete structural materials for major engineering such as long-span concrete bridge, marine concrete structures and infrastructure of high-speed rail. Additionally, RPC combined with functional fillers can serve as intrinsic self-sensing materials, providing real-time monitoring for large-scale building structures [4]. Moreover, this type of concrete can be applied to electromagnetic interference (EMI) shielding, deicing and electric heating systems [5–7].

Carbon nanofibers (CNFs) whose surface modified by oxidizer are easily dispersed in cement matrix [8]. This type of carbon nanofibers (CNFs) possesses excellent conduction and mechanical properties. Therefore, the addition of CNFs can decrease the resistivity and enhance the mechanical behavior of composites [9]. Cement-based materials with CNFs showed improvements of mechanical properties, conductivity and specific functional properties [10,11]. When being compared with short-cut carbon fibers (CFs), CNFs are more easily dispersed in cement matrix. Besides, the inner defects of CNFs are less than CFs. In comparison to carbon

* Corresponding author at: School of Civil Engineering, Harbin Institute of Technology, 150090 Harbin, China.
E-mail address: gaoxj@hit.edu.cn (X. Gao).

https://doi.org/10.1016/j.conbuildmat.2018.07.229
0950-0618/

nanotubes (CNTs), CNFs show numerous exposed edge planes along the surface. These exposed edge planes of CNFs possess advantageous chemical or physical interactions. Moreover, CNFs are produced at lower cost than CNTs. Being compared with metal fillers, CNFs show excellent corrosion resistance. Consequently, CNFs are regarded as excellent conductive fillers for making functional concrete [12].

Previous research pointed out that low water cement ratios lead to the decreased porosity for cement-based materials. Moreover, the conductive network of CNF-RPC was possibly improved by decreasing the water to cement ratio (w/c). Therefore, CNF-RPC with water cement ratios of less than 0.3 shows an obviously improved conductivity [9]. On the other hand, the addition of silica fume was useful to disperse CNFs due to the small particle size effect and the improved interfacial interaction between CNFs and RPC matrix [13]. Above all, RPC reinforced with CNFs may present ultra-high strength and excellent functional performance. However, little attention has been paid to the development of multi-functional RPC materials.

This paper investigated the multi-functional performance of CNF-RPC when CNFs was added by 0%, 0.25%, 0.5%, 1.0%, 1.5% and 2.0% of volume of the total binder. The measured properties included flexural and compressive strength, electrical resistivity, piezoresistivity and deicing performance. Finally, finite element analysis was applied to simulating the deicing process of CNF-RPC.

2. Experimental

2.1. Raw materials

The PR-19-XT-LHT-OX CNFs with a density of 2.1 g/cm^3 supplied by the Pyrograf Products, Inc was used in this study. The surface of CNFs was treated with oxidizer by producers for easily dispersing in cement matrix. This type of CNFs shows an average diameter of 149 nm and average length of 19 μm. Ordinary Portland cement with strength grade of 42.5 MPa in accordance with Chinese Standard GB175-2007 was used as cementitious material [14]. Silica fume with specific surface area of 15 m^2/g was used as a mineral admixture. The SiO_2 content of silica fume is more than 96% according to Chinese standard GB/T21236-2007 [15].

Quartz sand with two kinds of particle size of 0.35–0.59 mm and 0.15–0.297 mm were applied in preparing CNF-RPC. The quartz sand is composed of 99.6% SiO_2, 0.02% Fe_2O_3 and other ingredients. River sand with fineness modulus of 2.82 was used for preparing mortar samples. The flowability of fresh cement-based materials was adjusted by adding different dosage of polycarboxylate-based, high-range water-reducing agent (SP). The particle size distribution and chemical composition of cementitious materials are shown in Tables 1 and 2. In Table 2, R2O represents Na_2O and K_2O.

2.2. Mixing proportion and specimen preparation

To determine the mechanical and electrical properties of CNF-RPC, six groups of mixtures were prepared. Water to binder ratio by weight was kept at 0.20 in this study. The addition of silica fume, fine and coarse quartz sand of each group were 0.3, 0.22 and 0.88 by mass of cement respectively. CNFs were added by 0%, 0.25%, 0.5%, 1.0%, 1.5% and 2.0% by volume of the total cementitious materials respectively. The water reducing agent was added by 1.2–2.5% of the total weight of cementitious materials. These mixture types corresponding to different CNFs dosages were named by M1, M2, M3, M4, M5 and M6 respectively as shown in Table 3. On the other hand, CNFs added mortar and paste samples with water to binder ratio of 0.4 were also prepared and the cement-sand ratio of mortar was equal to that of RPC. Water-reducing agent was used to adjust the slump flow of CNF-RPC mixtures and mortars to reach around 180 mm for obtaining a good dispersion of CNFs [9,16]. For the same purpose, the slump flow of cement pastes containing CNFs was designed at around 200 mm.

Water-reducing agent was mixed uniformly in mixing water and then CNFs were added for a 3 min high speed stirring operation to obtain a homogeneous solution. A Hobart A200C (I.T.W. Inc., Chicago, America) planetary mixer was used to prepare fresh mortars with the same procedure. Firstly, cement (and silica fume if applicable) was added into the homogeneous solution containing CNFs and water-reducing agent for 3 min mixing at speed of about 140 rmp. Then, sand was added and mixed at a speed of about 285 rmp for another 3 min [17,18]. When the mortar mixing progress was completed, the mixture was poured into the oiled molds to form prism specimens with size of 35 mm × 35 mm × 55 mm and 210 mm × 100 mm × 50 mm. Samples with size of 35 mm × 35 mm × 55 mm were used to measure resistance and piezoresistivity. And plate specimens with size of 210 mm × 100 mm × 50 mm were selected to study the deicing performance. A concrete vibrator was used to facilitate the compaction and decrease air bubbles. The consolidated specimens were covered by plastic sheets for 2 days curing at room temperature and demolded. Then specimens were transferred to a standard fog room with temperature of 20 °C and relative humidity of above 95% for another

Table 3
Mixing parameters of CNF-RPC.

Types	Water reducing agent (%)	CNFs (%, by volume)	CNFs (%, by mass)
M1	1.2	0	0
M2	1.3	0.25	0.17
M3	1.5	0.5	0.34
M4	1.8	1.0	0.68
M5	2.0	1.5	1.02
M6	2.5	2.0	1.35

Table 1
Particle size distribution of raw materials (%).

Types	Particle size/um						
	0.3	0.6	1	4	8	64	360
Cement	0	0.33	2.66	15.01	28.77	93.59	100
Silica fume	31.2	58.3	82.3	100	100	100	100

Table 2
Chemical composition of cementitious materials.

Types	Chemical composition/%						
	SiO_2	Al_2O_3	Fe_2O_3	MgO	CaO	SO_3	R_2O
Cement	20.86	5.47	3.94	1.73	62.23	2.66	0.48
Silica fume	90	0.8	0.6	0.8	0.4	0	7.4

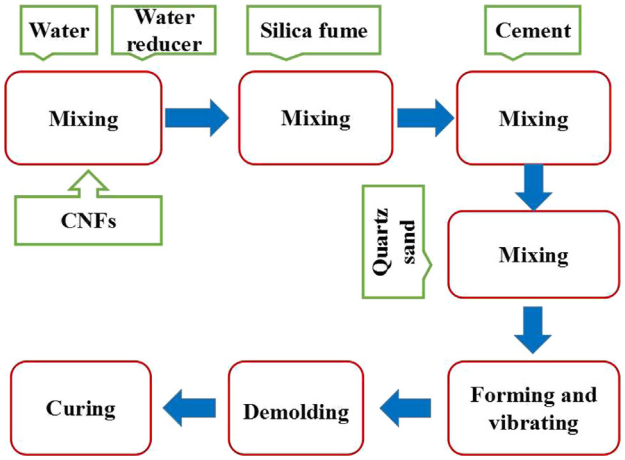

Fig. 1. Preparation process of CNF-RPC specimens.

26 days. The preparation process of CNF-RPC specimens is presented in Fig. 1.

2.3. Measurement methods

Electrical resistivity measurement was performed on 8 specimens for each group by using the embedded two-pole layout method at an AC voltage of 1 V with frequency of 10 kHz. AC electrical resistance was determined along the longitudinal axis direction of prisms. The electrodes were perpendicular to the longitudinal axis of specimen and the embedded electrodes were made of corrosion resistant 304 stainless steel mesh. Steel meshes with size of 30 mm × 50 mm and thickness of 0.4 mm were embedded in specimens with size of 35 mm × 35 mm × 55 mm. The distance between these two electrodes for every specimen was around 45 mm. Additionally, steel mesh with size of 80 mm × 65 mm and thickness of 0.4 mm was applied for specimens with size of 210 mm × 100 mm × 50 mm. TH2810D LCR digital electric bridge with testing frequency ranging from 100 Hz to 10 kHz was used to determine the AC resistance as shown in Fig. 2.

The piezoresistivity measurement was carried out by using an universal material testing machine with a maximum loading capacity of 100 kN and displacement loading rate of 0.5 mm/min as shown in Fig. 3. Each specimen underwent a preload of 1 kN before the piezoresistivity experiment to reduce the polarization effect. The stress (σ) used in piezoresistivity research under monotonic loading ranged from 0 to 15 MPa. Strain gauges were used to measure the compressive strain of every specimen. The strain

Fig. 2. Electrical resistance measurement.

gauges were attached to the middle positions of two opposite sides for every specimen and parallel to the loading direction. During the loading process, AC electrical resistance was simultaneously measured using the embedded two-pole layout as described earlier. Both electrical resistance and compressive strain were recorded once per second. Three specimens were tested for every group and the average value was determined. The average gage factor and linear degree of strain-sensing performance in each test were used to evaluate the self-sensing ability of CNF-RPC, CNFP and CNFM under the monotonic compressive loading. Before resistivity and piezoresistivity measurement, all specimens were dried in an oven at 60 °C for three days to minimize the polarization effect [9].

The fractional change in electrical resistance (*FCR*) can be given by

$$FCR = \frac{R - R_0}{R_0} \tag{1}$$

where R_0 is the initial resistance of the tested specimen before loading, R is the resistance during loading.

The gage factor (GF) was used to evaluate the sensitivity of the strain-sensing performance. GF is defined as the fractional change of resistance for per strain unit. ε means the compressive strain of CNF-RPC during the loading process. This parameter can be expressed as follows [19].

$$GF = \frac{FCR}{\varepsilon} \tag{2}$$

The linear degree (e_l) is usually used to calculate the nonlinear error of the strain-sensing performance for self-sensing materials as described by Formula (3). Δ_{max} is the maximum deviation between experimental value and linear fitting value of *FCR*. FCR_{max} is the maximum experimental value of *FCR*. The higher GF and lower linear degree reflect the better self-sensing property.

$$e_l = \pm \frac{\Delta_{max}}{FCR_{max}} \tag{3}$$

A DC power system with maximum voltage of 60 V was used to determine the deicing performance of CNF-RPC. The voltage used in this experiment was 30 V. DC current sensors and thermistors were used to collect the current and temperature during the deicing experiment. CNF-RPC plate samples for deicing performance were surrounded by polystyrene foam slab with only the top surface being exposed to the air. Fig. 4 shows the diagrammatic sketch of the deicing equipment. The deicing experiment was conducted in a sealed room with temperature of −20 °C.

2.4. Numerical modeling of deicing process

Finite element analysis software ANSYS 15.0 was used for the simulation analyses of deicing process. The temperature load varying with time was applied to the bottom surface of the ice model to simulate the heat transfer process from CNF-RPC plate. In the experiment, only the top surface of the ice block was exposed in the air. Therefore only the convection coefficient of heat transfer was applied to the top surface of the ice block as boundary condition in the simulation of the heat exchange between ice and air. Other four sides of the ice block were wrapped by thermal insulation material and the heat transfer coefficient is not considered in the simulation.

Assumptions for this modeling procedure included: the influence of wind speed on the heat transfer of the surface of the ice was ignored, the ice was regarded as a homogeneous object and the bottom side was fully contacted with the top surface of CNF-RPC specimen and the heat exchange between CNF-RPC and melted water was ignored.

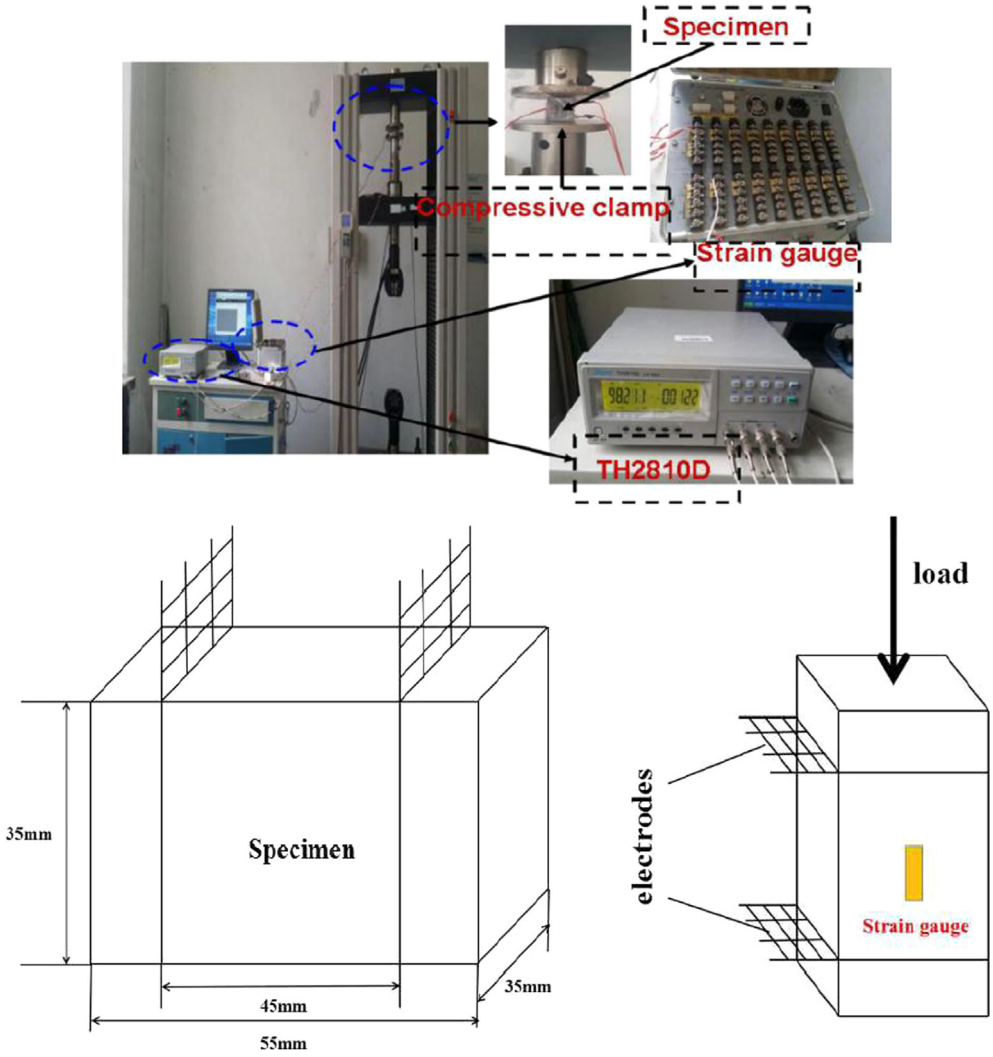

Fig. 3. Equipment for piezoresistivity test.

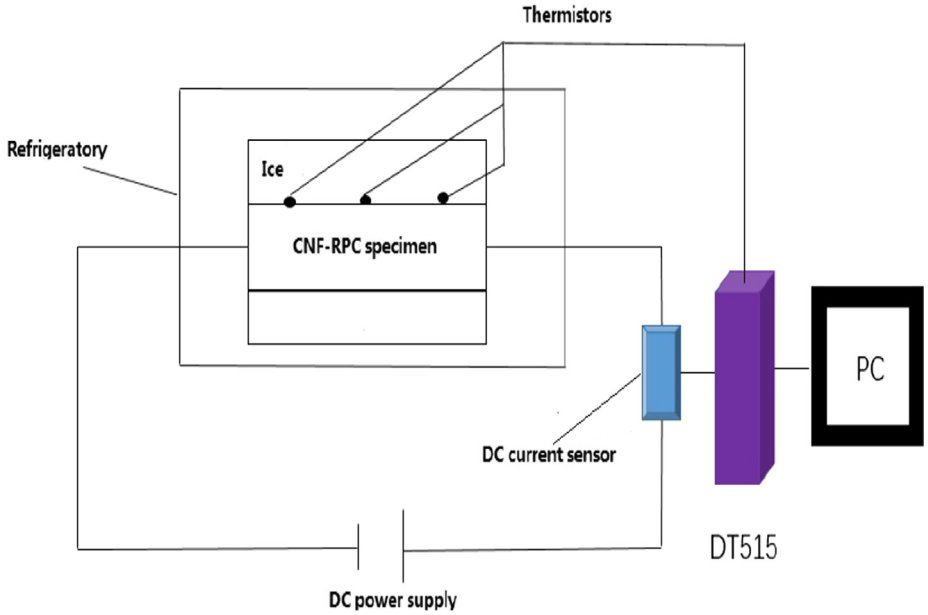

Fig. 4. Schematic of deicing experiment setup.

3. Results and discussions

3.1. Mechanical behaviors

Fig. 5 presents the test results of flexural strength and compressive strength of CNF-RPC samples with curing age of 28 days. It can be found that both flexural strength and compressive strength decreased firstly and then increased with the higher CNFs content. When the CNFs content reached 0.5%, the specimen presented the maximum mechanical strength. The increase of mechanical strength could be attributed to the effect of CNFs for bridging micro-cracks, filling the pores and accelerating the hydration reaction of the cement-based materials [11]. Moreover, CNFs could prevent the occurrence of micro-cracks and their free expansion [11,20,21]. The addition of CNFs reduced the porosities of the composites and refined the pore sizes, consequently enhanced the mechanical properties of CNF-RPC. Therefore, the mechanical strength of CNF-RPC increased with CNFs content ranging from 0% to 0.5%. On the other hand, it was reported that the existence of weak areas of CNFs and the inhibitory action on cement hydration induced by carbon nanomaterials possibly lead to a weaker strength [22,23]. More air bubbles are entrapped in cement paste due to the introduction of fibers or nano materials [24]. This can be used to explain that the strength was decreased when CNFs content increased from 0.5% to 2.0%.

3.2. Electrical resistance

Fig. 6 shows the conductive performance of CNF-RPC, CNFM and CNFP samples. The resistivity was decreased by the higher incorporation of CNFs for every group of cement-based materials. The resistance of CNF-RPC, CNFM and CNFP with CNFs dosages ranging from 0 to 0.5%, 1.5% and 1.5% respectively decreased slowly. With these incorporation levels, CNFs were isolated and no conductive chain was formed in cement matrix. The main electric conduction relies on the transfer of electrolyte ions [25]. Therefore, variable dosage of CNFs in these ranges had little influence on the conductivity. When CNFs continued to increase to a high level, CNFs formed a conductive link and led to the formation of a connected conductive path. Moreover, the spacing between adjacent fillers decreased, resulting in the improvement of conductive network [25]. Therefore, the resistance decreased obviously with the increasing content of CNFs. As observed in Fig. 6, CNF-RPC presented the optimal conductivity in these three CNFs cement-based materials. Being compared with CNFM, the lower w/c resulted in the reduction of porosity for CNF-RPC [3,4], being partly attributable to the improved conductive network of CNF-RPC.

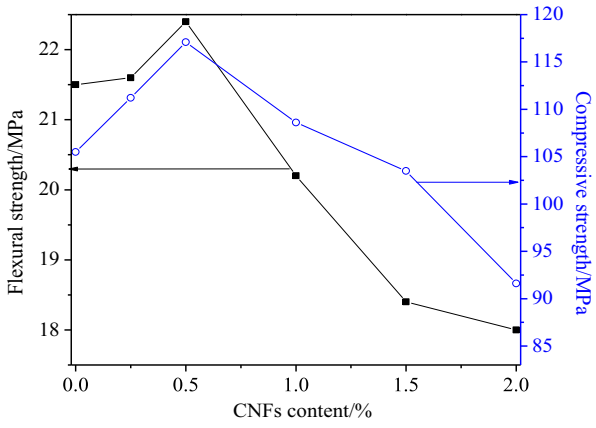

Fig. 5. Mechanical strength of CNF-RPC.

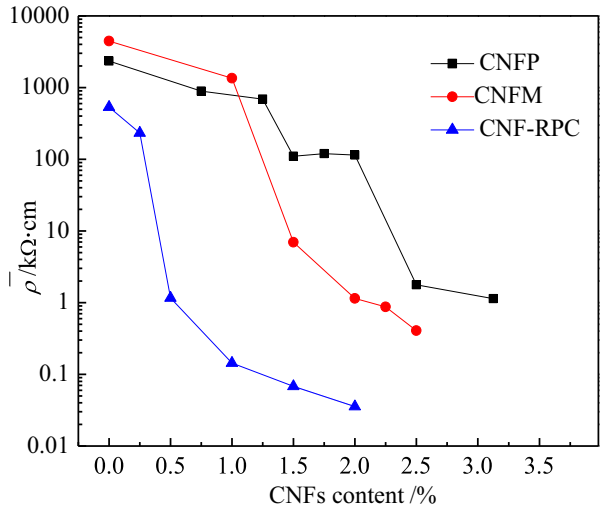

Fig. 6. Electrical resistivity of the CNFs cement-based composites.

Moreover, silica fume and quartz sand in CNF-RPC were useful to disperse CNFs and improve the conductive network [25–28]. In summary, the conductivity decreased in the order of CNF-RPC > CNFM > CNFP.

The microstructure of CNF-RPC, CNFM with 1.0% and 2.5% of CNFs are shown in Fig. 7 respectively. Fig. 6 illustrates that CNF-RPC with 1.0% of CNFs had a better conductivity than CNFM with 2.5% of CNFs. Fig. 7(a) demonstrates that CNFs are tightly wrapped by hydration products and thus the improved microstructure of CNF-RPC was induced. While the hydration products in CNFM looks very loose. As a result, CNF-RPC performed more excellent conductivity and mechanical behavior.

3.3. Piezoresistive performance

Fig. 8 shows the fractional change in resistance versus compressive strain for CNF-RPC, CNFM and CNFP specimens containing 0.5%, 2.25% and 2.25% of CNFs respectively. Table 4 gives the mean gage factor (GF) value and linear degree calculated for each group. When CNF-RPC containing less than 0.5% of CNFs and CNFM, CNFP containing less than 2.25% of CNFs, the resistance changed randomly with the axial compressive strain. Consequently, the piezoresistive results for those samples are not included in this paper. Of all groups, CNF-RPC showed the highest GF and lowest linear degree. The GF of CNF-RPC with 0.5% CNFs was more than 200 times of strain gauge. This might be attributed to the optimal CNFs dispersion, compact conductive network and dense RPC matrix, thus resulting in the excellent sensitivity and linearity [3–5]. However, CNFP showed the lowest sensitivity and linearity due to the worst conductivity and dispersion of CNFs.

Fig. 9 illustrates the evolution of electrical resistance with time of CNF-RPC with 0.5% and 1.0% content of CNFs respectively. These experiments were carried out under temperature of 20 °C. As shown in Fig. 9, the variation rate of resistance for these tested samples varied from −0.014% to 0.009%. It can be observed that the resistance rarely changed with the increasing time. According to the percolation theory, CNF-RPC consisting of 0.5% and 1.0% of CNFs reached the percolation threshold zone of conductivity [17,29,30]. Therefore, the tunneling effect played a critical role in conductivity, and ionic conduction was mainly eliminated by electronic conduction [29,30]. CNF-RPC is a kind of cement-based material with high compactness, therefore it possessed small amount of pore solution, thus resulting in the diminished polarization. The AC voltage method was able to decrease the polarization

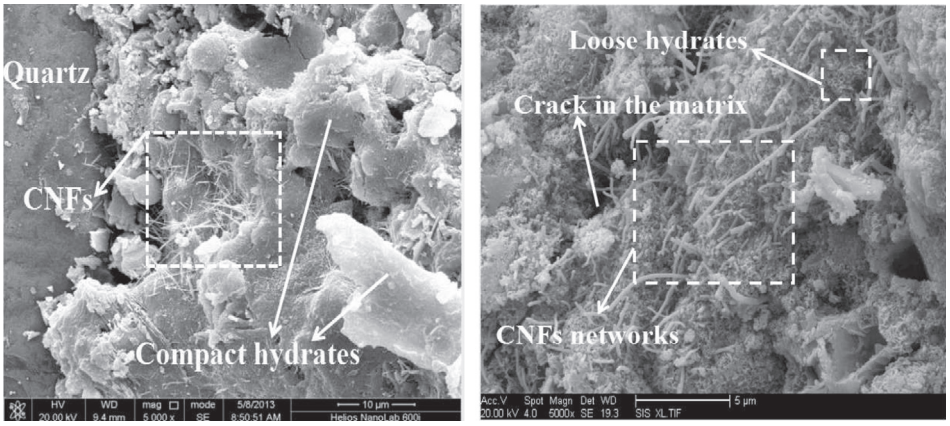

(a) CNF-RPC (b) CNFM

Fig. 7. Microstructure of CNF-RPC and CNFM.

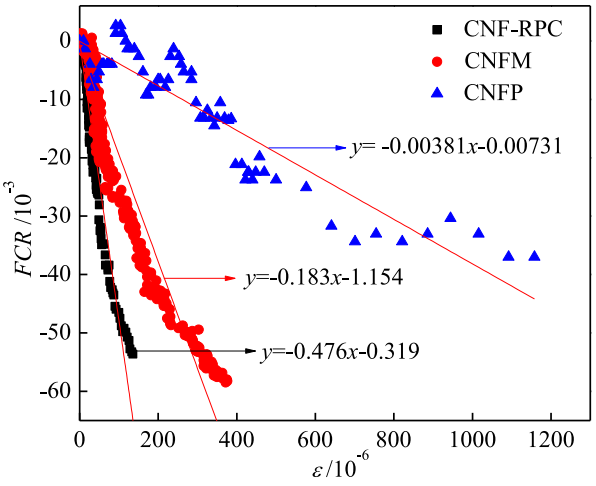

Fig. 8. Strain-sensing property of CNFs cement-based composites.

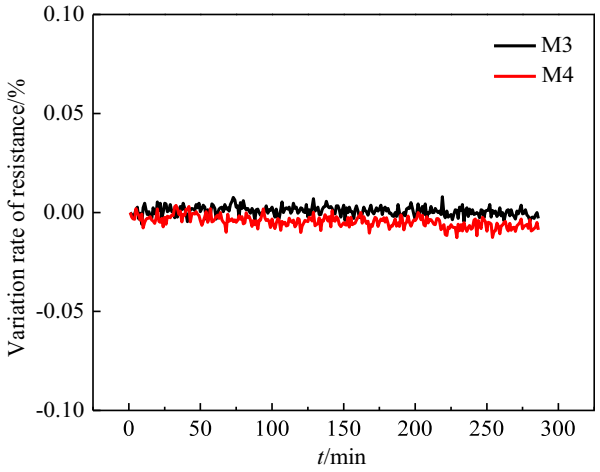

Fig. 9. Resistance fluctuation with time for CNF-RPC.

effect [26]. Moreover, the specimens were dried before this experiment, thus the reduction of free ions led to the decrease of polarization [26–28]. Therefore, it is indicated that CNF-RPC can be used as a sensor with a stable resistivity and self-sensing performance.

3.4. Deicing performance

Traditional snow removal by labor or machine and salt deicing chemical are labor-intensive and time-consuming. Moreover, these methods will cause damages to both the structures and the ecological environment. Self-heating concrete with good heating rate, high mechanical properties and stable electrical conductivity provides a potential substitute [31–33].

Fig. 10 presents the formation and accumulation of ice on CNF-RPC plates when exposed to a freezing chamber with temperature of −20 °C. It can be observed that ice accumulated to a high thickness for CNF-RPC containing 0.25% of CNFs, indicating little deicing

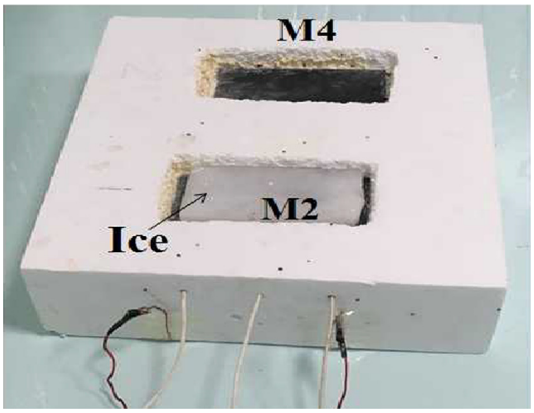

Fig. 10. Images of ice formation and accumulation on CNF-RPC plate.

Table 4
The fitting results of *FCR* and *ε*.

Equation	Type	*a*	*b*	Gage factor	Linear degree	R^2
$FCR = a\varepsilon + b$	CNF-RPC	−0.476	−0.319	476	2.35%	0.995
	CNFM	−0.183	−1.154	183	17.2%	0.972
	CNFP	−0.00381	−0.00731	38.1	23%	0.940

ability was obtained. On the other hand, ice was melted completely without delay for CNF-RPC containing 1.0% of CNFs. This is in accordance with a satisfactory conductivity for CNF-RPC containing 1.0% CNFs as shown in Fig. 6. Therefore, the addition of 1.0% CNFs in RPC achieved an excellent deicing performance, having a great potential for real structures in North China.

Fig. 11 illustrates the deicing ice mass for CNF-RPC samples containing different dosages of CNFs. It can be found that no detectable ice was deiced by the sample containing 0.25% CNFs. A deicing effect occurred when the addition of CNFs was higher than 0.5%. Deiced ice weight increased obviously with the increasing dosage of CNFs up to 1.0% and just a little increase was found when the CNFs content varied from 1.0% to 1.5%. The conductivity of CNFM (σ) is consisted of ionic conductivity (σ_i), hole conductivity (σ_h) and electronic conductivity (σ_e). Temperature of CNF-RPC tends to increase with the melting time and thus more pore solution is induced. The carrier conduction and streaming current of CNF-RPC containing water can be induced by the rise of ambient temperature [28]. Therefore, the enhanced conduction led to a drop in resistivity as illustrated in Fig. 12. As described in Formula (4), the electric heat is an inverse proportional to the resistance. In this equation, Q is the electric heat and U and R are the electrical voltage and the resistance of the tested specimen. According to this equation, the decrement of resistance led to the improvement of deicing rate for CNF-RPC specimens.

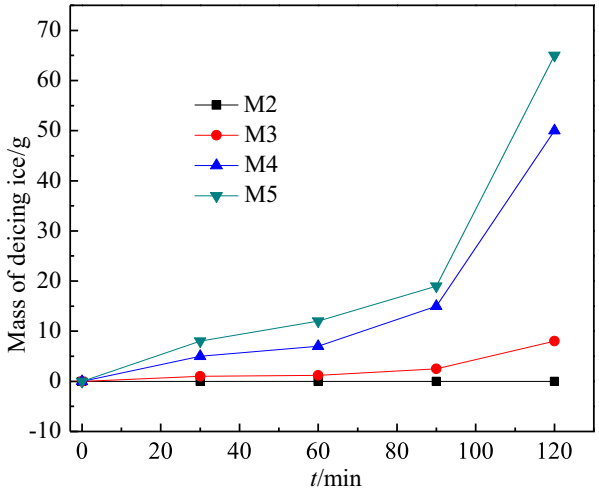

Fig. 11. Deicing ice mass with time.

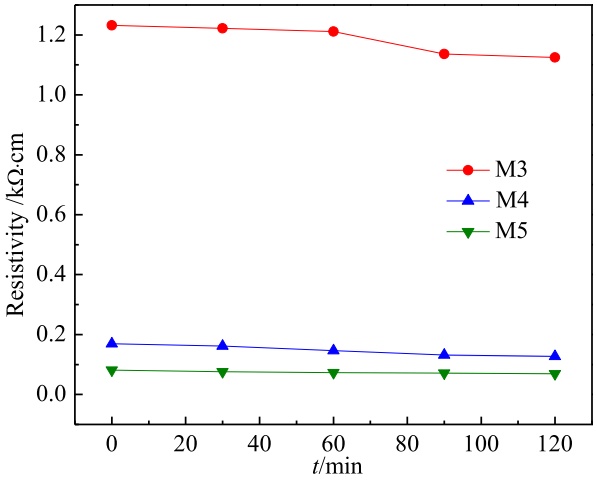

Fig. 12. Resistivity of CNF-RPC during the period of deicing ice.

Table 5
Heating power of self-heating cement-based materials with different conductive fillers.

Conductive fillers	Voltage (V)	Electric power/W	Reference
GP (5 vol% cement)	50	1.4	[30]
	100	6.6	[30]
	150	8.5	[30]
CNF (2 vol% cement)	50	3.6	[30]
	100	16.01	[30]
CNT (1.0 vol% cement)	50	14.9	[30]
SF (0.7 vol% cement)	50	285.7	[31]
GP (37 vol% cement)	50	3.0	[31]
CB (0.83 vol% cement)	50	2.1	[32]
CNF (1 vol% binder)	60	67.9	Present study
CNF (1.5 vol% binder)	60	82.3	Present study

$$Q = \frac{U^2}{R} \tag{4}$$

The heating power of self-heating cement-based materials with graphite powder (GP), steel fibers (SF), Carbon nanotubes (CNT), carbon black (GB), were added in Table 5 [31–33]. As illustrated, cement-based materials with 0.7 vol% of SFs showed the highest heating power. However, steel fibers in concrete were easily to corrode [34]. Except for cement-based materials containing steel fibers, CNF-RPC behaved the best heating power. Therefore, it was believed that CNF-RPC is suitable for deicing in real concrete structures and further studies should be carried out.

Fig. 13 indicates the finite element analysis results of the ice temperature on the top surface of CNF-RPC with 1.0% CNFs. The temperature decreased with the increasing distance between the top surface of CNF-RPC and the bottom surface of ice. When the conducting time ranged from 0 s to 3750.64 s, a significant weight of ice was melted. The melting of ice started from the bottom surface of the ice and then developed to a further distance. As the conducting time ranged from 3750.64 s to 7800 s, more than half of the ice was deiced. Fig. 13(d) indicated that there is little difference between the simulated values and experimental results. Therefore, this simulation method for deicing of CNF-RPC is acceptable.

4. Conclusion

This research developed one special kind of cement-based material with ultra-high-strength, self-sensing and deicing performance. The following conclusions can be obtained from the above experimental results.

1) Compressive and flexural strength of RPC increased firstly and then decreased with the higher dosage of CNFs. The maximum compressive and flexural strength reached 117.1 MPa and 22.4 MPa respectively when 0.5% of CNFs was added.
2) Resistance of CNF-RPC within the percolation threshold zone behaved stable with time. CNF-RPC presented a better conductivity and sensitivity than CNFM and CNFP. CNF-RPC with 0.5% CNFs (resistivity was 1.17 kΩ·cm) showed an excellent self-sensing performance with a high gage factor and stable sensing performance.
3) When CNFs reached 1.0% (resistivity was 0.144 kΩ·cm), CNF-RPC behaved a good deicing ability. The numerical simulation for deicing process provided a similar result to the experiment.

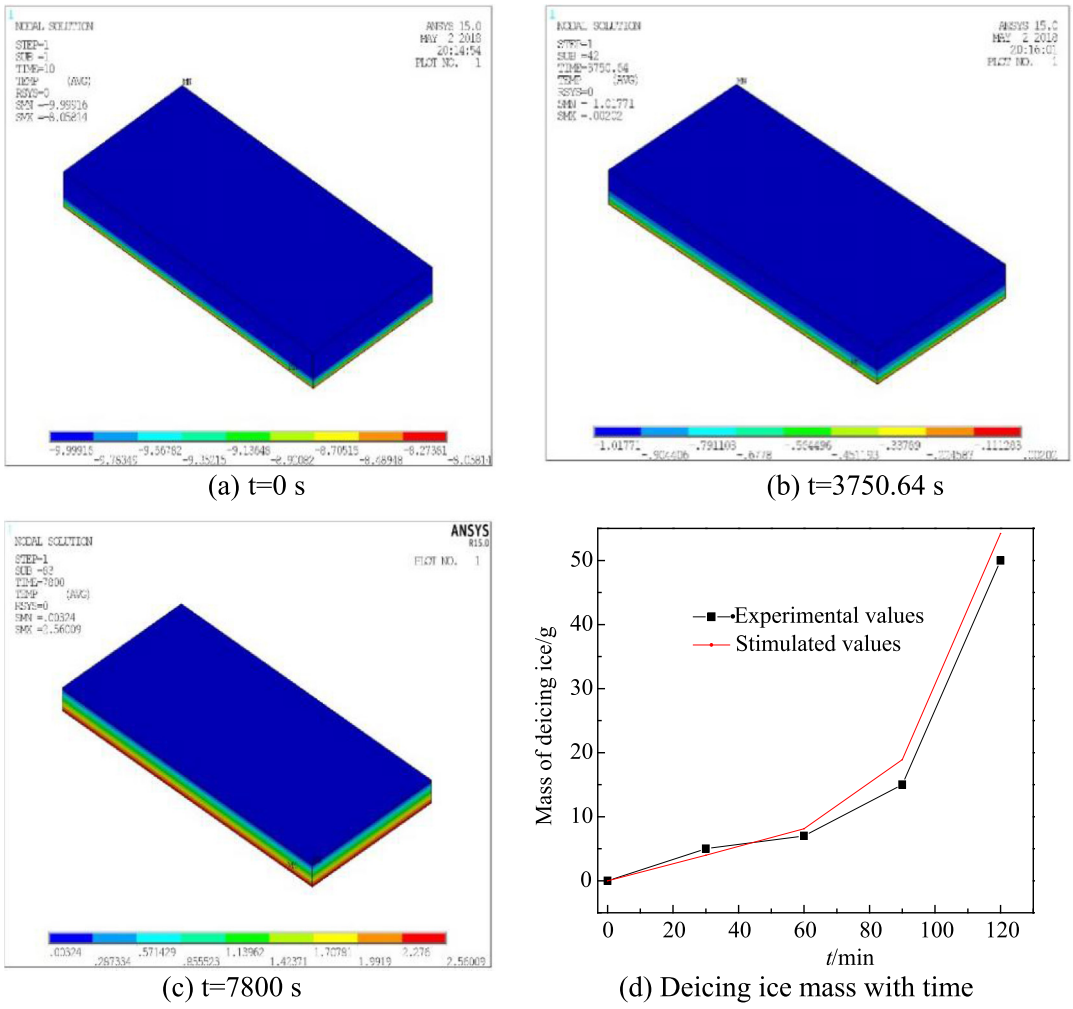

Fig. 13. Simulation of deicing process for CNF-RPC containing 1.0% CNFs.

Conflict of Interest

The authors declare no conflict of interest.

Acknowledgements

This work was sponsored by K.C. Wong Magna Fund in Ningbo University, the National Key R&D Program of China (No. 2017YFB0309901) and National Natural Science Foundation of China [No. 51478227 and No. 51778302].

References

[1] T. Zdeb, An analysis of the steam curing and autoclaving process parameters for reactive powder concretes, Constr. Build. Mater. 131 (2017) 758–766.
[2] A. Mo, S. El-Tawil, Z. Liu, W. Hansen, Effects of silica powder and cement type on durability of ultra-high performance concrete (UHPC), Cem. Concr. Compos. 66 (2016) 47–56.
[3] S. Dong, B. Han, et al., Electrically conductive behaviors and mechanisms of short-cut super-fine stainless wire reinforced reactive powder concrete, Cem. Concr. Compos. 72 (2016) 48–65.
[4] S. Dong, B. Han, et al., Microstructure related mechanical behaviors of short-cut super-fine stainless wire reinforced reactive powder concrete, Mater. Des. 96 (2016) 16–26.
[5] B.G. Han, Z. Li, et al., Reactive powder concrete reinforced with nano SiO_2-coated TiO_2, Constr. Build. Mater. 104–112 (2017).
[6] A. Mazzoli, V. Corinaldesi, et al., Effect of graphene oxide and metallic fibers on the electromagnetic shielding effect of engineered cementitious composites, J. Struct. Eng. 18 (2018).
[7] D. Micheli, A. Vricella, et al., Electromagnetic properties of carbon nanotube reinforced concrete composites for frequency selective shielding structures, Constr. Build. Mater. 131 (2017) 267–277.
[8] X. Gao, H. Wang, S. Li, L. Lu, Y. Mo, Piezoresistive effect of carbon nanofiber concrete exposed to different environmental conditions, Romanian J. Mater. 45 (4) (2015) 341–347.
[9] H. Wang, X. Gao, R. Wang, The influence of rheological parameters of cement paste on the dispersion of carbon nanofibers and self-sensing performance, Constr. Build. Mater. 134 (2017) 673–683.
[10] M.S. Konsta-Gdoutos, C.A. Aza, Self-sensing carbon nanotube (CNT) and nanofiber (CNF) cementitious composites for real time damage assessment in smart structures, Cem. Concr. Compos. 53 (2014) 162–169.
[11] K. Shimoda, T. Hinoki, A. Kohyama, Effect of carbon nanofibers (CNFs) content on thermal and mechanical properties of CNFs/SiC nanocomposites, Compos. Sci. Technol. 70 (2) (2010) 387–392.
[12] M. Ardanuy, M.A. Rodríguez-Perez, I. Algaba, Electrical conductivity and mechanical properties of vapor-grown carbon nanofibers/trifunctional epoxy composites prepared by direct mixing, Compos. Part B 42 (4) (2011) 675–681.
[13] F. Sanchez, C. Ince, Microstructure and macroscopic properties of hybrid carbon nanofiber/silica fume cement composites, Compos. Sci. Technol. 69 (7–8) (2009) 1310–1318.
[14] GB175-2007, Common Portland cement. China Standard Press, 2007(in Chinese).
[15] GB/T21236-2007, Silica fume from electric-furnace. China Standard Press, 2007(in Chinese).
[16] F. Zou, H. Tan, et al., Effect of sodium gluconate on dispersion of polycarboxylate superplasticizer with different grafting density in side chain, J. Ind. Eng. Chem. 55 (2017) 91–100.
[17] H. Li, H. Xiao, J. Ou, Electrical property of cement-based composites filled with carbon black under long-term wet and loading condition, Compos. Sci. Technol. 68 (9) (2008) 2114–2119.
[18] B. Han, J. Ou, Embedded piezoresistive cement-based stress/strain sensor, Sens. Actuators, A 138 (2) (2007) 294–298.

[19] O. Galao, F.J. Baeza, E. Zornoza, P. Garcés, Strain and damage sensing properties on multifunctional cement composites with CNF admixture, Cem. Concr. Compos. 65 (6) (2015) 1222–1228.
[20] G.G. Tibbetts, M.L. Lake, K.L. Strong, B.P. Rice, A review of the fabrication and properties of vapor-grown carbon nanofiber/polymer composites, Compos. Sci. Technol. 67 (7–8) (2007) 1709–1718.
[21] D. Gao, Y.L. Mo, L.M. Peng, Mechanical and electrical properties of carbon-nanofiber self-consolidating concrete, Earth and Space 366 (2014) 2577–2585.
[22] B. Zhang, F. Kang, et al., Recent advances in electrospun carbon nanofibers and their application in electrochemical energy storage, Prog. Mater. Sci. 76 (2016) 319–380.
[23] Y. Dai, M. Sun, C. Liu, Z. Li, Electromagnetic wave absorbing characteristics of carbon black cement-based composites, Cem. Concr. Compos. 32 (7) (2010) 508–513.
[24] L. Zhang, S. Ding, et al., Effect of characteristics of assembly unit of CNT/NCB composite fillers on properties of smart cement-based materials, Compos. Part A 109 (2018) 303–320.
[25] H. Wang, X. Gao, J. Liu, Effects of salt freeze-thaw cycles and cyclic loading on the piezoresistive properties of carbon nanofibers mortar, Constr. Build. Mater. 177 (20) (2018) 192–201.
[26] J. Cao, D.D.L. Chung, Electric polarization and depolarization in cement-based materials, studied by apparent electrical resistance measurement, Cem. Concr. Res. 34 (3) (2004) 481–485.
[27] S. Wen, D.D.L. Chung, Effect of stress on the electric polarization in cement, Cem. Concr. Res. 31 (31) (2001) 291–295.
[28] S. Wen, D.D.L. Chung, Electric polarization in carbon fiber-reinforce cement, Cem. Concr. Res. 31 (1) (2001) 141–147.
[29] M. Sun, Z. Li, Q. Mao, D. Shen, A study on thermal self-monitoring of carbon fiber reinforced concrete, Cem. Concr. Res. 29 (5) (1999) 769–771.
[30] H. Yokota, E. Kato, M. Iwanami, Chloride-induced corrosion of reinforcement and its effect on performance of structures, Int. J. Model. Ident. Control 7 (7) (2009) 179–184.
[31] J. Gomis, O. Galao, Self-heating and deicing conductive cement. Experimental study and modeling, Constr. Build. Mater. 75 (2015) 442–449.
[32] S. Wang, S. Wen, D.D.L. Chung, Resistance heating using electrically conductive cements, Adv. Cem. Res. 16 (4) (2004) 161–166.
[33] M. Sun, Y. Wu, et al., Deicing concrete pavement containing carbon black/carbon fiber conductive lightweight concrete composites, Int. Conf. Transport. Inf. Safety (2011) 662–668.
[34] K. Tang, Stray current induced corrosion of steel fiber reinforced concrete, Cem. Concr. Res. 100 (2017) 445–456.